



Light-Sheet Scattering Microscopy to Visualize Long-Term Interactions Between Cells and Extracellular Matrix

Xiangda Zhou¹, Renping Zhao¹, Archana K. Yanamandra^{1,2}, Markus Hoth¹ and Bin Qu^{1,2*}

¹ Biophysics, Center for Integrative Physiology and Molecular Medicine (CIPMM), School of Medicine, Saarland University, Homburg, Germany, ² INM-Leibniz Institute for New Materials, Saarbrücken, Germany

OPEN ACCESS

Edited by:

Christoph Wülfling,
University of Bristol, United Kingdom

Reviewed by:

John Robert James,
University of Warwick,
United Kingdom
Jörg Renkawitz,
Ludwig Maximilian University of
Munich, Germany

*Correspondence:

Bin Qu
bin.qu@uks.eu

Specialty section:

This article was submitted to
T Cell Biology,
a section of the journal
Frontiers in Immunology

Received: 03 December 2021

Accepted: 11 January 2022

Published: 28 January 2022

Citation:

Zhou X, Zhao R, Yanamandra AK,
Hoth M and Qu B (2022) Light-Sheet
Scattering Microscopy to Visualize
Long-Term Interactions Between
Cells and Extracellular Matrix.
Front. Immunol. 13:828634.
doi: 10.3389/fimmu.2022.828634

Visualizing interactions between cells and the extracellular matrix (ECM) mesh is important to understand cell behavior and regulatory mechanisms by the extracellular environment. However, long term visualization of three-dimensional (3D) matrix structures remains challenging mainly due to photobleaching or blind spots perpendicular to the imaging plane. Here, we combine label-free light-sheet scattering microscopy (LSSM) and fluorescence microscopy to solve these problems. We verified that LSSM can reliably visualize structures of collagen matrices from different origin including bovine, human and rat tail. The quality and intensity of collagen structure images acquired by LSSM did not decline with time. LSSM offers abundant wavelength choice to visualize matrix structures, maximizing combination possibilities with fluorescently-labelled cells, allowing visualizing of long-term ECM-cell interactions in 3D. Interestingly, we observed ultrathin thread-like structures between cells and matrix using LSSM, which were not observed by normal fluorescence microscopy. Transient local alignment of matrix by cell-applied forces can be observed. In summary, LSSM provides a powerful and robust approach to investigate the complex interplay between cells and ECM.

Keywords: light-sheet, scattering microscopy, label-free, ECM-cell interaction, long-term

INTRODUCTION

Under physiological conditions, immune cells and tumor cells encounter complex and dynamic three-dimensional (3D) environments. To maintain 3D environments, extracellular matrix (ECM) composed of fibrous mesh networks serves as one main structural component. Concerning immune surveillance, interaction of ECM with immune cells plays an essential role in tuning physiological responses (1). It is reported that *in vivo* macrophages structurally form vascular mimicry channels, which are ultrastructurally different from an endothelial vasculature (2). *In vitro* evidence shows that fast migrating primary human CD8⁺ T cells preferably migrate into and expand the existing channels in 3D collagen matrices, facilitating migration of subsequent immune cells (3). These channels could presumably contribute to metastasis of tumor cells (4). In case the channels in ECM

are too narrow, the width could serve as a speed limiting factor to restrain the migration of immune cells (5). Migration of cells in ECM per se results in structural changes in ECM (3) and such structural changes may result in different outcomes of immune surveillance. To investigate this, long-term visualization of ECM-cell interaction with defined and controllable features is needed.

However, long-term visualization of ECM structures remains technically challenging. One of the most applied approaches is to label the matrix protein of interest fluorescently (6). Unfortunately, due to photobleaching, this method does not offer a satisfactory solution for long-term visualization. There are numerous other approaches well established to visualize fibrillar collagen, such as electron microscopy (7) and two-photon imaging with second harmonic generation (SHG) (8). Although electron microscopy enables visualization of matrix structure with a high resolution, it cannot be applied for live cell imaging. SHG can detect living cells *in vivo* and *in vitro* (9, 10), and can be combined with fluorescence labelling (11) to observe ECM-cell interactions, which is especially advantageous for intravital imaging. Femto- or picosecond-pulsed high-power laser is required for SHG (12). The effect of this high-power laser on fast moving immune cells for long-term visualization is not yet reported. Another confocal-based method called confocal reflection microscopy utilizes the light reflected by the fibrous structure of the matrix (13), offering a possibility to visualize collagen structure without fluorescence, which can also be combined with long-term live cell imaging. However, with confocal reflection microscopy, the subset of fibrous structures perpendicular to the imaging plane cannot be detected due to a blind spot, resulting in incomplete information in 3D structure of the reconstructed networks (14).

Light can be scattered during its propagation in the sample in an inelastic or elastic manner. Inelastic scattering occurs when the light is scattered off at molecular bonds, resulting in change in energy and the corresponding frequency (15). The spectrum of inelastic scattering is utilized to characterize chemical composition of samples in 3D, as for example performed with Raman scattering (16). In contrast, when the light is scattered by spatial structures, there is no energy loss in the scattered light. This process is termed as elastic scattering. Several recent studies have used elastically scattered light with light-sheet microscopy to visualize plant roots in transparent soil or in gels (17), freshly-excised tissues *ex vivo* (18) or blood cells *in vivo* (19) without fluorescent labeling.

In this paper, we verified the label-free light-sheet scattering microscopy (LSSM) as a robust approach to visualize ECM structures without blind spot and photobleaching. Non-fluorescently labeled cells can be also visualized by LSSM. LSSM is particularly advantageous to visualize long-term cell-ECM interactions, and to analyze cell behavior adapted to dynamic ECM meshworks. Interestingly, applying LSSM we observed thin thread-like structure between cells and matrix, which could not be observed by normal fluorescence microscopy. Furthermore, LSSM can be used to characterize forces exerted on the matrix by the embedded cells.

MATERIALS AND METHODS

Reagents

The following reagents were used in this work: Atto Fluor 647 NHS-Ester (Succinimidylester), Atto Fluor 488 NHS-Ester (Succinimidylester), CellTrace CFSE Cell Proliferation Kit (ThermoFisher Scientific), and CellTrace Calcein Red-Orange AM (ThermoFisher Scientific). RatCol Rat Tail Collagen (4 mg/ml), FibriCol Type I Collagen Solution (bovine, 10 mg/ml) and VitroCol Type I Collagen Solution (Human, 3 mg/ml) were obtained from Advanced BioMatrix.

Cell Preparation and Cell Culture

Human primary CD4⁺ and CD8⁺ T cells were negatively isolated using CD4 or CD8 T Cell Isolation Kit Human (Miltenyi) from peripheral blood mononuclear cells (PBMCs) of healthy donors (20). T cells were stimulated with Dynabeads Human T-Activator CD3/CD28 (ThermoFisher Scientific) and cultured in AIM V Medium (ThermoFisher Scientific) with 10% FCS (ThermoFisher Scientific) at a density of 2×10^6 cells/ml. Human pancreatic beta cells 1.4E7 were purchased from Merck and cultured in RPMI-1640 medium (ThermoFisher Scientific) supplemented with 2 mM glutamine, 1% penicillin-streptomycin plus 10% FCS. SK-MEL-5 cells were cultured in MEM medium (ThermoFisher Scientific) containing 10% FCS and 1% penicillin-streptomycin. K562-pCasper cells were cultured in RPMI-1640 medium (ThermoFisher Scientific) supplemented with 1.25 mg/ml G418, 1% penicillin-streptomycin and 10% FCS. All cells were cultured at 37°C with 5% CO₂.

Preparation of Collagen Matrices

Collagen solutions were prepared as previously described (21). Briefly, chilled 10× PBS was added to collagen stock solution prior to neutralization with 0.1 M NaOH. The neutralized collagen solution was further diluted to the desired concentrations with 1× PBS for structure visualization or with AIMV medium for live cell imaging. The collagen was then sucked into a glass capillary and kept at 37°C with 5% CO₂ for 40 min for polymerization.

Fluorescent Labeling of Collagen Fibers

After polymerization, the collagen rod was pushed out of the capillary carefully and immersed in the freshly made Atto Fluor 647 NHS-Ester or Atto Fluor 488 NHS-Ester solution (50 μg/ml) for 10 min at room temperature, followed by three times washing with 1× PBS for 5 min. For live cell imaging, additional steps were required as previously reported (6). Briefly, the Atto Fluor 488 NHS-ester-stained collagen was dissolved in acetic acid (20 mM) at 4°C. Then the acid-dissolved fluorescently labeled collagen was mixed with non-labeled collagen in a ratio between 1:25-1:50. The cell pellet was resuspended in this mixed collagen solution and polymerization was conducted as described above.

Light-Sheet Microscopy

A Zeiss Lightsheet.Z1 light-sheet microscope was used for all experiments. The imaging chamber was assembled according to

the manufacturer's instructions. For LSSM, the combination of 445 nm laser (power 0.2%), LBF 405/488/561/640, SBS LP 490-BP 420-470 with an exposure time of 30 ms was used if not mentioned otherwise. The samples were illuminated from one side if not mentioned otherwise. For fluorescence imaging modality, the following settings were used: 561 nm laser (power 0.5%), LBF 405/488/561/640, SBS LP 560-LP 585 with an exposure time of 100 ms for calcein-AM red-orange; 488 nm laser (power 1.0%), LBF 405/488/561/640, SBS LP 490-BP 505-545, with an exposure time of 30 ms was used for Atto 488; 638 nm laser (power 0.5%), LBF 405/488/561/640, SBS LP 560-LP 660 was used for Atto 647; 488 nm laser (power 0.5%), LBF 405/488/561/640, SBS LP 510-BP 525-565 with an exposure time of 80 ms for CFSE. Time lapse with Z-stacks (step-size: 0.4-1.5 μm as indicated in the figure legends) was conducted with a 20 \times objective at 37°C. The intervals and total length of visualization are stated in the corresponding figure legend.

For live cell imaging, the cells were loaded with calcein-AM red-orange (0.5 μM) at 37°C for 30 min or with CFSE (5 μM) at room temperature for 15 min. CFSE-stained cells were recovered in the incubator for 24 hours prior to imaging. The cells were centrifuged, and the pellet was resuspended in the collagen solution followed by 40 min-polymerization and 1 hour recovery in the incubator. 3D reconstruction, maximum intensity projection (MIP) and channel merge were generated with Zen (Zeiss). Tracking of collagen matrix displacement was manually carried out with the ImageJ plugin MTrackJ as reported elsewhere (22). Manders' coefficients were analyzed using ImageJ plugin JACoP (Just Another Colocalization Plugin) (23). Sample drift during image acquisition was corrected with Correct Drift in Imaris with the options for 'the entire image and all objects' and 'translational and rotational drift'.

RESULTS

LSSM Is a Label-Free Robust Method to Visualize Collage Structure

In order to visualize long-term cell-ECM interactions in larger 3D structures, we looked for a label-free method based on light-sheet microscopy. We therefore investigated whether elastically scattered light can be used to visualize ECM structures. To this end, we prepared type I bovine collagen samples in glass capillaries and visualized the collagen sample with various lasers (405 nm, 445 nm, 488 nm, 514 nm, 561 nm, 638 nm) in combination with different block filters, beam splitters and detection filters as summarized in **Supplementary Figure 1A**. The acquired images show that among 216 possible combinations, the collagen structure were seen in 35 combinations (**Supplementary Figure 1B**), which share a common feature: the combination of the block filter, the beam splitter and the detection filter does not exclude the wavelength of the excitation laser. In comparison, many of these working combinations do exclude theoretical emission wavelength of the auto-fluorescence, which could be excited by the corresponding

laser. Our findings indicate that the structure of matrices are visualized by the elastically scattered light. This technique is hereinafter referred to as light-sheet scattering microscopy (LSSM). Of note, during acquisition, a very low laser power and short exposure time were applied, suggesting that photocytotoxicity induced by LSSM is very low if not negligible, and that a fast scan speed can be achieved.

To verify whether the matrix structure acquired by LSSM reflects the original structure of the matrix, we fluorescently labeled human collagen and scanned the same samples using LSSM and fluorescence microscopy simultaneously. The results show that the fibrous structures and reconstructed 3D structures visualized by LSSM and fluorescence microscopy are very similar (**Figure 1A**). We noticed that the intensity profile of the fibers do not always match between LSSM and fluorescence microscopy (**Movies 1-3**), i.e. the brightest fibers in the former are not necessarily also the brightest ones in the latter. We postulated that it could be owed to uneven staining efficiency. To further examine overlapping of fibers visualized by LSSM and fluorescence microscopy, we analyzed Manders' coefficients. M1 (scattering over fluorescence) is 0.756 ± 0.051 and M2 (fluorescence over scattering) is 0.725 ± 0.068 (**Figure 1A**). To examine the robustness of LSSM, we also analyzed the collagen from different origin such as bovine (**Figure 1B**) and rat tail (**Figure 1C**). Manders' coefficients are 0.689 ± 0.038 (M1) and 0.643 ± 0.022 (M2) for bovine samples, 0.577 ± 0.129 (M1) and 0.696 ± 0.064 (M2) for rat tail samples. The results show that LSSM reliably obtained the key structural features of collagen matrices from different sources, with different concentrations and pore sizes.

No Blind Spot and No Photobleaching in LSSM

In confocal reflection microscopy, a blind spot has been reported, where around half of the fibers, which are vertically oriented above 50 degrees from the focal plane, missing in image data acquired by confocal reflection imaging modality (14). We therefore explored whether LSSM has the same limitation. For LSSM, we chose dual side fusion mode, in which the samples were illuminated from both the left and the right side sequentially and the images from both sides were merged to generate the final image (**Figure 2A**). We noticed that although not many, a few fibers did appear in images from only one side (**Figure 2B**, Scattering Mode, insets 1-2), indicating that in LSSM modality illumination from only one side could leave a few fibers undetected, presumably due to the orientation of the fibers. Interestingly, a few fibrous structures were detected only in LSSM (**Figure 2B**, inset 1, comparing Scattering Mode and Fluorescence Mode). This implies that for thin fibrous structures, LSSM could be advantageous compared to fluorescence microscopy.

Photobleaching is a major bottle neck for long-term visualization, at least for fluorescence microscopy. We next analyzed photobleaching in LSSM. Images of fluorescently labeled collagen matrices were acquired using LSSM and fluorescence imaging modality every 30 sec for 6 hours. Time

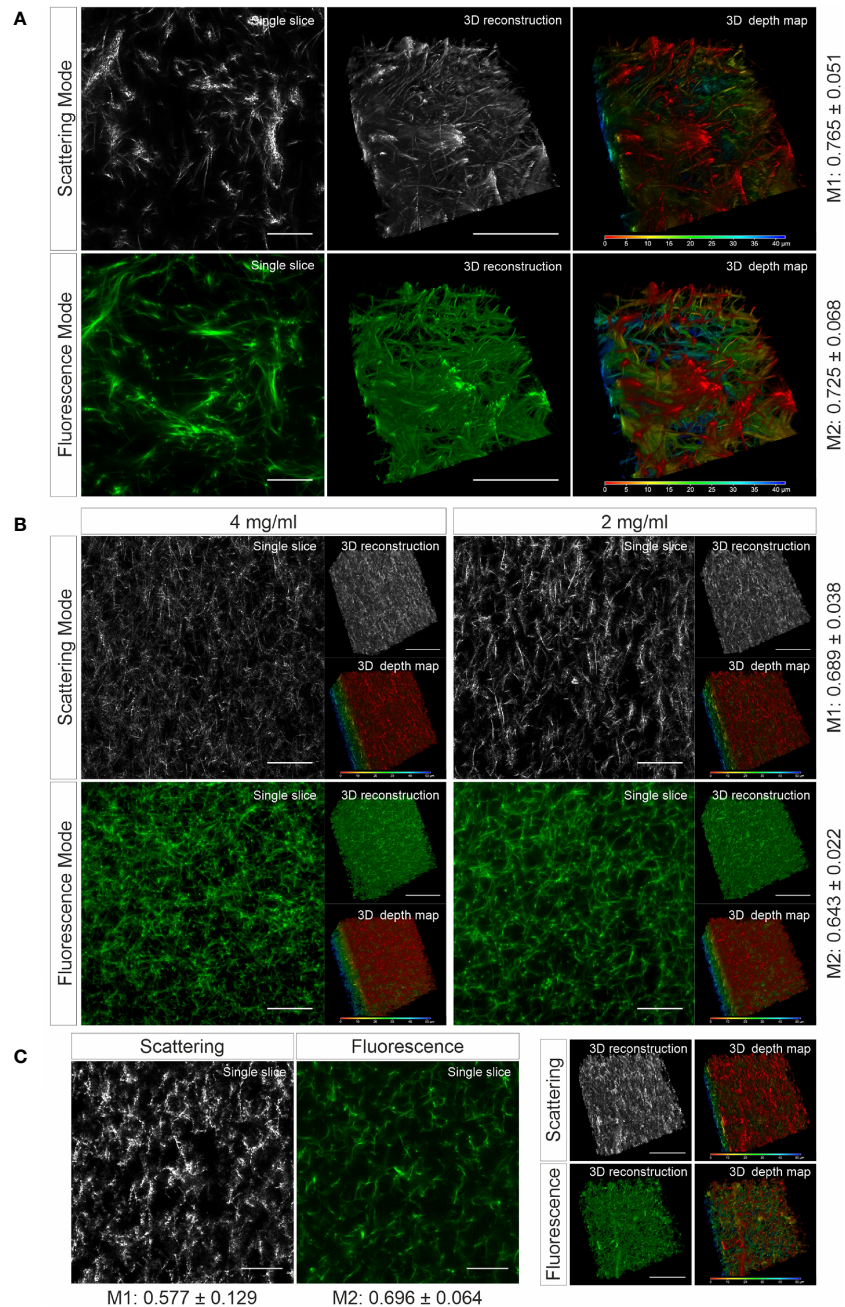


FIGURE 1 | Collagen structures visualized by LSSM. Collagen from human (A), (2mg/ml), bovine (B), (2 and 4 mg/ml) or rat tail (C), (2mg/ml) was used. Collagen was fluorescently labeled with Atto 488. Z-stacks with step-size of $0.4 \mu\text{m}$ for 95 slices (A) or for 119 slices (B, C) were acquired. Scale bars are $40 \mu\text{m}$. Representative images from at least three independent experiments are shown. Mander's coefficients (M1: scattering over fluorescence, M2: fluorescence over scattering) were quantified from 3 (A) or 4 (B, C) independent experiments.

lapse images and the analysis show a substantial photobleaching in fluorescence microscopy, while no photobleaching was detected in LSSM (Figures 2C, D). This technical advantage of LSSM enables reliable long-term visualization of dynamic change of matrix structures as well as matrix-cell interaction.

Application of LSSM to Investigate ECM-Cell Interaction

Characterization of ECM-cell interaction is essential to understand the behavior of cells in 3D. We examined whether LSSM could be applied to meet this purpose. We first loaded SK-

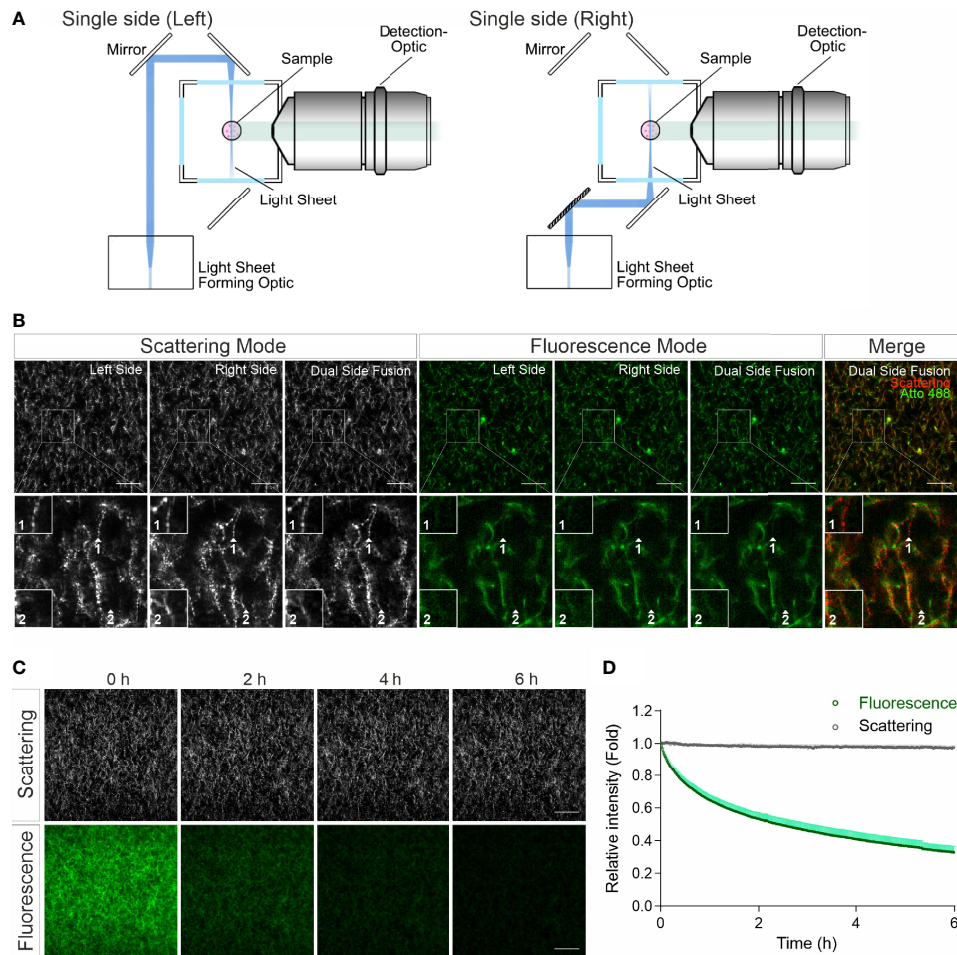


FIGURE 2 | LSSM avoids photobleaching and blind spot problems. **(A)** Sketch for single side illumination. **(B)** Comparison of images acquired by LSSM and fluorescence microscopy. Rat tail collagen (2 mg/ml) was fluorescently labeled with Atto 488. Images from single side illumination and the merged images of both sides (dual side fusion) are shown. Z-stacks with step-size of 1 μm for 51 slices were obtained with LSSM and fluorescence mode concurrently at 37°C. **(C, D)** Signal intensity obtained by LSSM is not reduced with time. Bovine collagen (2 mg/ml) was labeled with Atto 647. Z-stacks with step-size of 0.621 μm for 50 slices were obtained with LSSM and fluorescence mode subsequently at 37°C every 30 sec for 6 hours. Scale bars are 40 μm . Quantification is shown as Mean \pm SEM. Representative images from at least three independent experiments are shown.

MEL-5 cells, a melanoma cell line, with calcein-AM red-orange and embedded the cells in the Atto 488-labeled collagen matrix. Z-stacks of the samples were taken at 37°C every 30 sec for about half an hour. Interestingly, in LSSM, the SK-MEL-5 cells were also detected, and the cells could be morphologically distinguished from the mesh network of collagen matrix (**Figure 3A**). Unexpectedly, highly dynamic filamentous structures linking the cells and the mesh network were detected in LSSM, which could not be detected by fluorescence modality (**Figure 3A** and **Movie 4**, highlighted by the arrowheads), implying that those structures are unlikely to originate from the collagen matrix but rather from the SK-MEL-5 cells. Time lapse images from LSSM show that these dynamic filamentous structures were formed between SK-MEL-5 cells and the matrix when the cells moved away from the matrix

(**Figure 3A** (7.5 min and 8 min) and **Movie 4**), and also formed between SK-MEL-5 cells when the two cells migrated apart (**Figure 3A** (20 min and 20.5 min) and **Movie 4**). Another example of these ultrathin structures is shown in **Supplementary Figure 2A** and **Movie 5**.

To identify whether these filamentous structures are unique to SK-MEL-5 cells, we used 1.4E7 cells, a human pancreatic beta cell line. Again, highly dynamic ultrathin filamentous structures between the cells and the mesh network were observed in LSSM, which could not be detected by fluorescence modality (**Figure 3B** inset and **Movie 6**, highlighted in the upper frame). In addition, distortion of the matrix caused by cell contraction was also observed in both imaging modalities (**Movie 6**, highlighted in the lower frame). 3D reconstructions and the depth map (pseudocolors are assigned to different depth) further reveal that

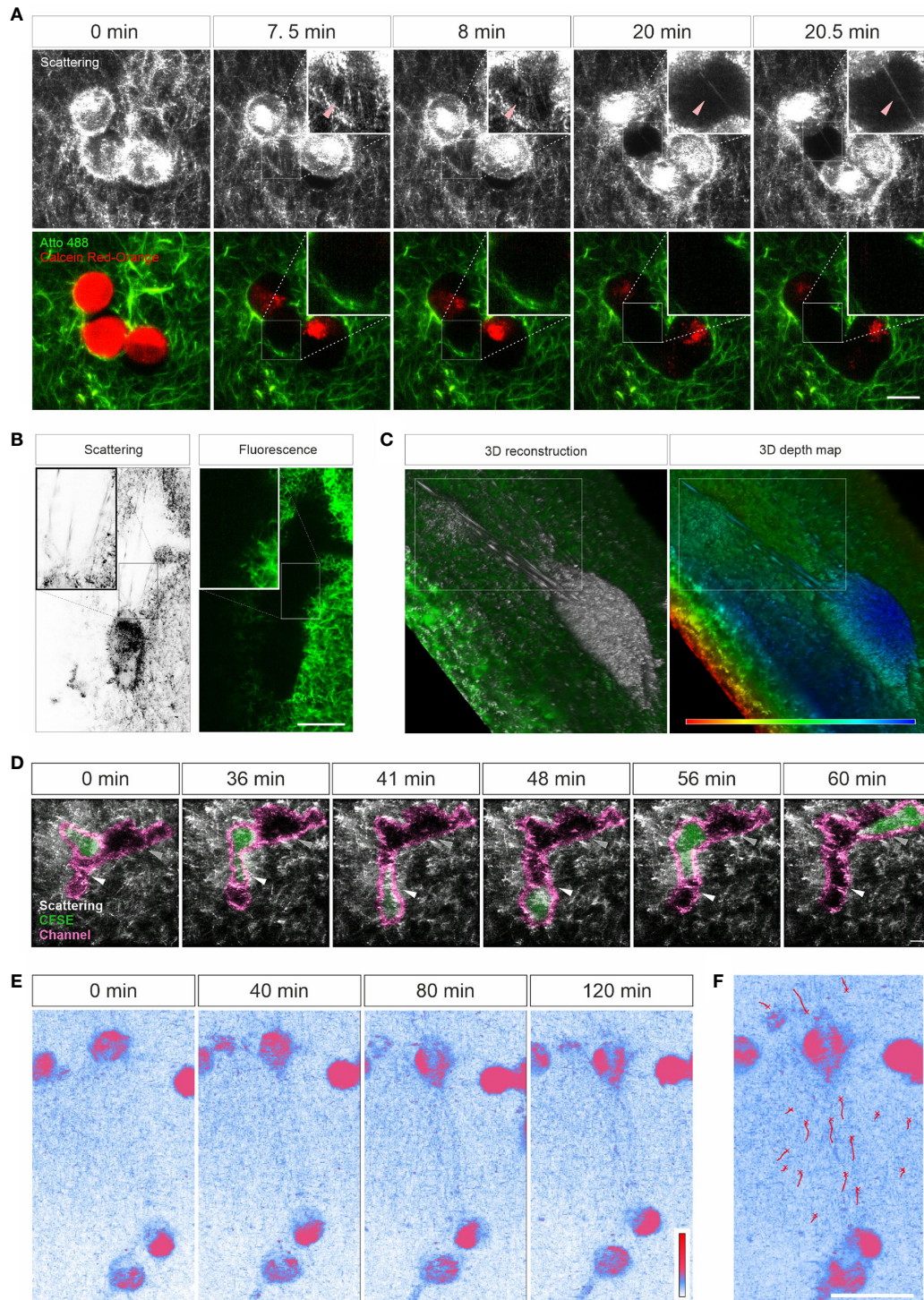


FIGURE 3 | Live cell imaging with LSSM. **(A–C)** Ultrathin filamentous structures observed with LSSM. Rat tail collagen (2 mg/ml) was fluorescently labeled with Atto 488. Calcein-AM red-orange loaded SK-MEL-5 cells **(A)** or non-labeled 1.4E7 human pancreatic beta cells **(B, C)** were embedded in the matrix. Z-stacks with step-size of 0.82 μm for 52 slices **(A)** or 0.418 μm for 82 slices **(B, C)** were obtained using LSSM and fluorescence modality concurrently at 37°C every 30 sec for 35.5 min **(A)** or every 20 sec for 10 min **(B, C)**. **(D)** T cells enter channels in ECM. Primary human CD4⁺ T cells were loaded with CFSE and were embedded in the collagen matrices (Bovine collagen, 2 mg/ml). Z-stacks with step-size of 1.5 μm for 70 slices were obtained using LSSM and fluorescence modality concurrently at 37°C every 1 min for 1 hour. **(E, F)** Cell-induced displacement of collagen fibers. Non-labeled SK-MEL-5 cells were embedded in rat tail collagen (2 mg/ml). Z-stacks with step-size of 1 μm for 295 slices were obtained using LSSM at 37°C every 1 min for 2 hours. Scale bars are 20 μm . Representative events from three independent experiments are shown.

those filamentous structures were parallelly orientated in 3D and could be traced back to the cell body (Figure 3C). These findings indicate that these LSSM-identified filamentous structures could play an essential role in regulating ECM-cell interaction and cell-cell interaction, especially in 3D environments.

Next, we examined whether LSSM is suitable to visualize fast migrating immune cells and their interaction with ECM. We loaded primary human CD4⁺ T cells with CFSE, and visualized T cell migration in label-free 3D collagen matrices using LSSM in combination with fluorescence microscopy. Channels in collagen matrices were detected in LSSM as reported previously using fluorescence microscopy (3). We observed that after entry into the channel, in this example the CD4⁺ T cell first chose the segment with a narrower width (Figure 3D, highlighted by the white arrowhead, Movie 7), expanded the channel and then reversed the direction and advanced to the other segmentation (Figure 3D, highlighted by the grey arrow head, Movie 7). A similar migration was observed also for CD8⁺ T cells (Supplementary Figure 2B and Movie 8). These results show that LSSM is a powerful tool to characterize matrix structure-regulated migration behavior.

Mechanical forces are an essential factor to modulate cell function and the interplay between ECM and cells. When cells exert mechanical forces on the matrix, deformation of matrix is induced and can be used to characterize the mechanical forces exerted by the cells (24, 25). Using LSSM, this deformation could

be observed as shown in Movie 6. We further examined whether this deformation could be characterized with LSSM. To this end, we embedded not-fluorescently labeled SK-MEL-5 cells in collagen matrices and acquired images every 1 min for 2 hours. Time lapse images show that with LSSM, SK-MEL-5 cells can be distinguished from the ECM based on their morphology. Interestingly, collagen fibers between two SK-MEL-5 cells were reorientated and aligned towards the cells at a macroscopic length scale (Figures 3E, F and Movie 9). These findings indicate that LSSM can be applied to characterize cell-applied mechanical forces.

Finally, we examined long-term imaging. Using LSSM combining with fluorescence microscopy we visualized migration of calcein-AM red-orange-labeled primary human CD4⁺ T cells in collagen at 37°C every 3 minutes for 8 hours. As shown in Figure 4A and Movie 10, primary human CD4⁺ T cells remained mobile till the end of the observation. Quantification of the cell velocity shows that T cell velocity at 5 h was not differed from that at 1 h and 3 h, and T cell velocity at 7 h remained comparable as that at 1 h and slightly higher than that at 3 h (Figure 4B). A strong bleach of the dye in T cells was observed after 7 hours, nevertheless the T cell migration was not altered as identified by the signal from LSSM (Movie 10). We then attempted for measurements for even longer time. To be able to monitor viability of the cells, we used K562-pCasper cells, a human chronic myelogenous leukemia cell line stably

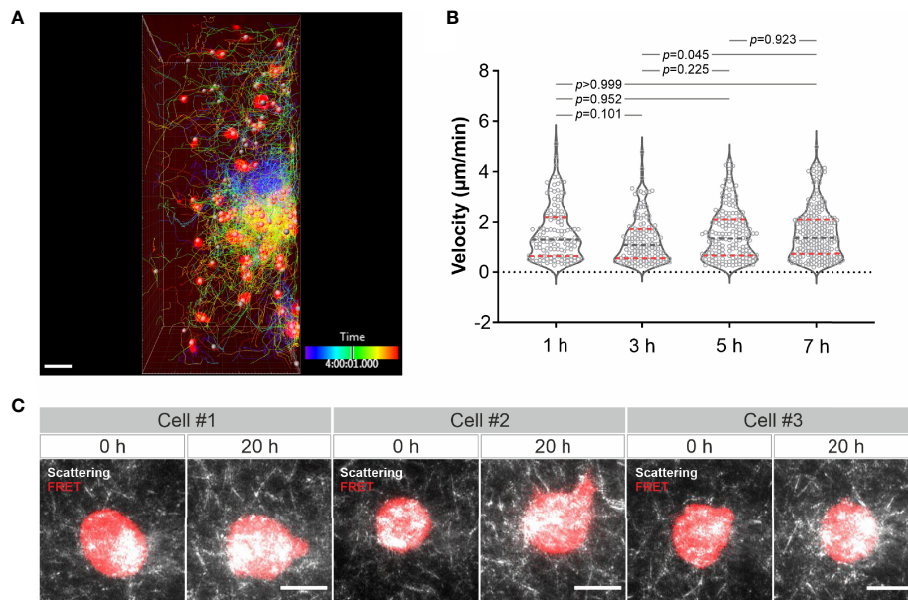


FIGURE 4 | Long-term visualization of cell-ECM interaction. **(A)** T cell migration in long-term visualization. Calcein-AM red-orange loaded primary human CD4⁺ T cells were embedded in the collagen matrices (Bovine collagen, 2 mg/ml). Z-stacks with step-size of 2 µm for 98 slices were obtained using LSSM and fluorescence modality concurrently at 37°C every 3 min for 10 hours. A drift correction was performed. T cells were automatically tracked. A maximum intensity projection (MIP) of all the 98 slices is shown. Scale bars are 40 µm. **(B)** Quantification of T cell velocity. To analyze cell velocity, T cells in five frames before and after each time point were tracked and the mean velocity during this time (30 min) was calculated. For time point 1h, 3h, 5h and 7h, 127 cells, 144 cells, 167 cells and 214 cells were analyzed. Multiple comparisons in ordinary one-way ANOVA was used for *p* values. Gray dashed lines are the median. Red dashed lines are the ends of the first and third quartiles. **(C)** K562 cells stably expressing pCasper was embedded in the collagen matrices (Bovine collagen, 2 mg/ml). Z-stacks with step-size of 2 µm for 75 slices were obtained using LSSM and FRET fluorescence modality simultaneously at 37°C every 5 min for 20 hours. A maximum intensity projection (MIP) from three exemplary cells is shown. Scale bars are 10 µm.

expressing pCasper, which is an apoptosis reporter composed of a GFP-RFP FRET pair linked by a caspase recognition site DEVD. The FRET signal will be abruptly lost when the cells undergo apoptosis or necrosis (26). K562-pCasper cells embedded in collagen were visualized at 37°C every 5 minutes for 20 hours. FRET signal shows that most of the K562-pCasper cells (14 out of 17) stayed alive (no abrupt loss of FRET signal) till the end of the observation (**Figure 4C**). The K562 cells made protrusions and deformation of the matrix by the cells was also visible (**Movie 11**). Thus, we conclude that the photocytotoxicity of LSSM is negligible for long-term visualization, at least up to 20 hours.

DISCUSSION

In this work, we report that ECM meshwork can be reliably visualized by LSSM. One major advantage of LSSM is that the signal intensity does not decline over time, which makes LSSM a powerful tool for long-term measurements. Another advantage of LSSM is that in contrast to reflection confocal microscopy, there is no blind spot, allowing label-free reconstruction of 3D ECM structures without discontinuous artefacts. In addition, LSSM can detect thin fibrous structures generated by cells. For ECM-cell interaction, this robust method can be combined with fluorescence modality to reveal more details of cell-ECM interactions. For chemotaxis, theoretically chemokine gradients can be built by adding chemokines into the bath solution in the sample chamber.

LSSM utilizes the light scattered sideways by the collagen fibers, which is detected by the objective perpendicular to the imaging plane. Here, the imaging plane is illuminated by a thin sheet of light, the incidence angle of which is parallel to the imaging plane. In comparison, images taken by confocal reflection microscopy are formed from the light reflected by the collagen fibers. Therefore, the fibers vertically orientated to the imaging plane are not detected, leading to an artefact that 3D reconstructed matrix structures seem to be aligned to the imaging plane. For LSSM, the possibility for a total reflection by a fiber leading to a blind spot is theoretically extremely low. As shown in our results, the fibrous structures oriented to all directions were observed, and no discontinuation of vertically oriented fibers in 3D reconstructed networks were detected. In addition, since LSSM uses the scattered light, the signal intensity is not reduced with time. Thus, LSSM is shown to be a reliable label-free method to visualize mesh networks without photobleaching, which is especially advantageous for long-term measurements.

Nevertheless, there are several potential disadvantages of LSSM. First and foremost, due to the assembly of the incubation chamber no oil-immersion objective can be used, therefore the resolution for LSSM is not high (~0.7 μm for an 20 \times objective or ~0.45 μm for an 40 \times objective), which would limit the application of LSSM for revealing ultrastructural details of ECM or the cells. In this aspect, confocal-based approaches would be more advantageous, especially for short term from minutes up to an

hour or so as beautifully shown by numerous works using confocal reflection microscopy with label-free collagen (27–29) or using confocal fluorescence microscopy with fluorescently labeled collagen (30). In addition, LSSM-obtained fibers could appear pixelated compared to images obtained by fluorescence microscopy. These pixelated structures are not a reflection of the microstructure of matrix fibers, but rather an artefact, which could be owed to light scattering-influencing physical properties of the fibers, e.g. angles of fiber curvature. It could happen that at discontinuous derivable points or segments, light might not be scattered properly.

Using LSSM, we unexpectedly observed ultrathin filamentous structures between diverging cells or between matrices and the moving cells. Since these structures were not detected in fluorescence microscopy and the collagen was fluorescently labelled, the ultrathin filamentous structures are likely to originate from the cells. This postulation is further supported by our observation that these structures appear to be generated between diverging cells. Nevertheless, as the collagen fibers could be too thin to be stained for fluorescent microscopy, a possible origin of these ultrathin structures from collagen cannot be fully excluded. These ultrathin structures could be derived from plasma membrane with or without architectural support of cytoskeleton. Several types of thin cell protrusions are reported such as invadopodia and microtentacles. Invadopodia are thin, short, actin-rich structures, which are formed to protrude into the ECM (31). Microtentacles are needle-like structures formed by microtubules and intermediate filaments, which are found in many tumor cells, especially in circulating tumor cells, suggestively contributing to cancer metastasis (32). Whether the origin, generation mechanism and functions of the thin structures detected by LSSM share common features with invadopodia or microtentacles require further investigation.

Mechanical interplay between cells and matrix plays a pivotal role for cell migration, differentiation, self-organization, and activation of cells (24, 25, 33–35). Cell-cell distant mechanical communications *via* matrix is essential for cell self-assembly (25). Traction forces generated by cells lead to matrix deformation, enabling force transmission to distant cells. In a 3D scenario, traction forces generated by a single cell or spheroid can be well determined by traction force microscopy, which measures the displacement of microbeads evenly distributed in the matrix (36, 37). We observed that collagen fibers were aligned between two SK-MEL-5 cells. Emerging evidence shows that aligned matrix potentiates cell migration to a fast mode (34). Tracking migrating immune cells in 3D matrices using LSSM can address the question that whether this cell-induced transient local alignment of matrix could be used by immune cells as directional cues to quickly find their target cells.

In summary, we present LSSM as a reliable and robust tool for long-term visualization of ECM-cell interactions. Using this assay, important scientific questions can be addressed. These include measurements of cell-cell mechanical interactions, of long-range traction force transmission, and of dynamic ECM-immune cell interactions, which may change migration patterns or even search strategies.

DATA AVAILABILITY STATEMENT

The datasets presented in this study can be found in online repositories. The names of the repository/repositories and accession number(s) can be found below:

Figure 1 “LSSM for long-term ECM-cell interaction_Fig.1”, Mendeley Data, V1, doi: 10.17632/v5259wncpw.1.

Figure 2 “LSSM for long-term ECM-cell interaction_Fig.2”, Mendeley Data, V1, doi: 10.17632/6vphrtcvpz.1.

Figure 3 and Figure 4 “LSSM for long-term ECM-cell interaction_Fig.3+Fig. 4”, Mendeley Data, V1, doi: 10.17632/wjv83t7264.1.

AUTHOR CONTRIBUTIONS

XZ performed most experiments and the corresponding analyses if not mentioned otherwise. RZ performed the experiments and analysis for **Figure 2D**. AKY helped to prepare the samples. MH helped with data interpretation and provided critical feedback on all aspects of the project. BQ generated concepts, designed experiments, and wrote the manuscript. All authors contributed to the writing of the manuscript and provided advice. All authors contributed to the article and approved the submitted version.

REFERENCES

- Winkler J, Abisoye-Ogunniyan A, Metcalf KJ, Werb Z. Concepts of Extracellular Matrix Remodelling in Tumour Progression and Metastasis. *Nat Commun* (2020) 11:5120. doi: 10.1038/s41467-020-18794-x
- Barnett FH, Rosenfeld M, Wood M, Kioussis WB, Usui Y, Marchetti V, et al. Macrophages Form Functional Vascular Mimicry Channels In Vivo. *Sci Rep* (2016) 6:36659. doi: 10.1038/srep36659
- Sadjadi Z, Zhao R, Hoth M, Qu B, Rieger H. Migration of Cytotoxic T Lymphocytes in 3D Collagen Matrices. *Biophys J* (2020) 119:2141–52. doi: 10.1016/j.bpj.2020.10.020
- Wagenblast E, Soto M, Gutierrez-Angel S, Hartl CA, Gable AL, Maceli AR, et al. A Model of Breast Cancer Heterogeneity Reveals Vascular Mimicry as a Driver of Metastasis. *Nature* (2015) 520:358–62. doi: 10.1038/nature14403
- Renkawitz J, Kopf A, Stopp J, de Vries I, Driscoll MK, Merrin J, et al. Nuclear Positioning Facilitates Amoeboid Migration Along the Path of Least Resistance. *Nature* (2019) 568:546–50. doi: 10.1038/s41586-019-1087-5
- Doyle AD. Fluorescent Labeling of Rat-Tail Collagen for 3D Fluorescence Imaging. *Bio Protoc* (2018) 8:e2919. doi: 10.21769/BioProtoc.2919
- Starborg T, Kalson NS, Lu Y, Mironov A, Cootes TF, Holmes DF, et al. Using Transmission Electron Microscopy and 3View to Determine Collagen Fibril Size and Three-Dimensional Organization. *Nat Protoc* (2013) 8:1433–48. doi: 10.1038/nprot.2013.086
- Chen X, Nadiarynkh O, Plotnikov S, Campagnola PJ. Second Harmonic Generation Microscopy for Quantitative Analysis of Collagen Fibrillar Structure. *Nat Protoc* (2012) 7:654–69. doi: 10.1038/nprot.2012.009
- Friedl P, Wolf K, von Andrian UH, Harms G. Biological Second and Third Harmonic Generation Microscopy. *Curr Protoc Cell Biol* (2007) Chapter 4: Unit 4 15. doi: 10.1002/0471143030.cb0415s34
- Campagnola PJ, Clark HA, Mohler WA, Lewis A, Loew LM. Second-Harmonic Imaging Microscopy of Living Cells. *J Biomed Opt* (2001) 6:277–86. doi: 10.1117/1.1383294
- Lau D, Garçon F, Chandra A, Lechermann LM, Aloj L, Chilvers ER, et al. Intravital Imaging of Adoptive T-Cell Morphology, Mobility and Trafficking Following Immune Checkpoint Inhibition in a Mouse Melanoma Model. *Front Immunol* (2020) 11:1514. doi: 10.3389/fimmu.2020.01514

FUNDING

This project was funded by the Deutsche Forschungsgemeinschaft (SFB 1027 Project A2 to BQ, A11 to MH, and GZ: INST 256/419-1 FUGG to MH), and by Bundesministerium für Bildung und Forschung (031L0133 to MH).

ACKNOWLEDGMENTS

We thank the Institute for Clinical Hemostaseology and Transfusion Medicine for providing donor blood; Carmen Hässig, Cora Hoxha, Sandra Janku, and Gertrud Schäfer for excellent technical help; Carsten Kummerow for technical help in light-sheet microscopy.

SUPPLEMENTARY MATERIAL

The Supplementary Material for this article can be found online at: <https://www.frontiersin.org/articles/10.3389/fimmu.2022.828634/full#supplementary-material>

- Wolf K, Alexander S, Schacht V, Coussens LM, von Andrian UH, van Rheenen J, et al. Collagen-Based Cell Migration Models *In Vitro* and *In Vivo*. *Semin Cell Dev Biol* (2009) 20:931–41. doi: 10.1016/j.semcdb.2009.08.005
- Brightman AO, Rajwa BP, Sturgis JE, McCallister ME, Robinson JP, Voytik-Harbin SL. Time-Lapse Confocal Reflection Microscopy of Collagen Fibrillogenesis and Extracellular Matrix Assembly *In Vitro*. *Biopolymers* (2000) 54:222–34. doi: 10.1002/1097-0282(200009)54:3<222::AID-BIP80>3.0.CO;2-K
- Jawerth LM, Munster S, Vader DA, Fabry B, Weitz DA. A Blind Spot in Confocal Reflection Microscopy: The Dependence of Fiber Brightness on Fiber Orientation in Imaging Biopolymer Networks. *Biophys J* (2010) 98:L1–3. doi: 10.1016/j.bpj.2009.09.065
- Ostertag E, Stefanakis M, Rebner K, Kessler RW. Elastic and Inelastic Light Scattering Spectroscopy and Its Possible Use for Label-Free Brain Tumor Typing. *Anal Bioanal Chem* (2017) 409:6613–23. doi: 10.1007/s00216-017-0614-1
- Jones RR, Hooper DC, Zhang L, Wolverson D, Valev VK. Raman Techniques: Fundamentals and Frontiers. *Nanoscale Res Lett* (2019) 14:231. doi: 10.1186/s11671-019-3039-2
- Yang Z, Downie H, Rozbicki E, Dupuy LX, MacDonald MP. Light Sheet Tomography (LST) for *In Situ* Imaging of Plant Roots. *Opt Express* (2013) 21:16239–47. doi: 10.1364/OE.21.016239
- Nguyen CD, O’Neal PK, Kulkarni N, Yang E, Kang D. Scattering-Based Light-Sheet Microscopy for Rapid Cellular Imaging of Fresh Tissue. *Lasers Surg Med* (2021) 53:872–9. doi: 10.1002/lsm.23361
- McKay GN, Niemeier RC, Castro-Gonzalez C, Durr NJ. Scattering Oblique Plane Microscopy for *In-Vivo* Blood Cell Imaging. *BioMed Opt Express* (2021) 12:2575–85. doi: 10.1364/BOE.422993
- Kummerow C, Schwarz EC, Bufe B, Zufall F, Hoth M, Qu B. A Simple, Economic, Time-Resolved Killing Assay. *Eur J Immunol* (2014) 44:1870–2. doi: 10.1002/eji.201444518
- Schoppmeyer R, Zhao R, Hoth M, Qu B. Light-Sheet Microscopy for Three-Dimensional Visualization of Human Immune Cells. *J Vis Exp* (2018) 136:57651. doi: 10.3791/57651
- Meijering E, Dzyubachyk O, Smal I. Methods for Cell and Particle Tracking. *Methods Enzymol* (2012) 504:183–200. doi: 10.1016/B978-0-12-391857-4.00009-4

23. Bolte S, Cordelieres FP. A Guided Tour Into Subcellular Colocalization Analysis in Light Microscopy. *J Microsc* (2006) 224:213–32. doi: 10.1111/j.1365-2818.2006.01706.x
24. Underwood CJ, Edgar LT, Hoving JB, Weiss JA. Cell-Generated Traction Forces and the Resulting Matrix Deformation Modulate Microvascular Alignment and Growth During Angiogenesis. *Am J Physiol Heart Circ Physiol* (2014) 307:H152–64. doi: 10.1152/ajpheart.00995.2013
25. Davidson CD, Wang WY, Zaimi I, Jayco DKP, Baker BM. Cell Force-Mediated Matrix Reorganization Underlies Multicellular Network Assembly. *Sci Rep* (2019) 9:12. doi: 10.1038/s41598-018-37044-1
26. Backes CS, Friedmann KS, Mang S, Knorck A, Hoth M, Kummerow C. Natural Killer Cells Induce Distinct Modes of Cancer Cell Death: Discrimination, Quantification, and Modulation of Apoptosis, Necrosis, and Mixed Forms. *J Biol Chem* (2018) 293:16348–63. doi: 10.1074/jbc.RA118.004549
27. Zanotelli MR, Goldblatt ZE, Miller JP, Bordeleau F, Li J, Vanderburgh JA, et al. Regulation of ATP Utilization During Metastatic Cell Migration by Collagen Architecture. *Mol Biol Cell* (2018) 29:1–9. doi: 10.1091/mbc.E17-01-0041
28. Salvermoser M, Pick R, Weckbach LT, Zehrer A, Lohr P, Drechsler M, et al. Myosin 1f Is Specifically Required for Neutrophil Migration in 3D Environments During Acute Inflammation. *Blood* (2018) 131:1887–98. doi: 10.1182/blood-2017-10-811851
29. Wolf K, Te Lindert M, Krause M, Alexander S, Te Riet J, Willis AL, et al. Physical Limits of Cell Migration: Control by ECM Space and Nuclear Deformation and Tuning by Proteolysis and Traction Force. *J Cell Biol* (2013) 201:1069–84. doi: 10.1083/jcb.201210152
30. Welf ES, Driscoll MK, Dean KM, Schafer C, Chu J, Davidson MW, et al. Quantitative Multiscale Cell Imaging in Controlled 3D Microenvironments. *Dev Cell* (2016) 36:462–75. doi: 10.1016/j.devcel.2016.01.022
31. Murphy DA, Courtneidge SA. The 'Ins' and 'Outs' of Podosomes and Invadopodia: Characteristics, Formation and Function. *Nat Rev Mol Cell Biol* (2011) 12:413–26. doi: 10.1038/nrm3141
32. Killilea AN, Csencsits R, Le E, Patel AM, Kenny SJ, Xu K, et al. Cytoskeletal Organization in Microtentacles. *Exp Cell Res* (2017) 357:291–8. doi: 10.1016/j.yexcr.2017.05.024
33. Francois J, Kandasamy A, Yeh YT, Schwartz A, Ayala C, Meili R, et al. The Interplay Between Matrix Deformation and the Coordination of Turning Events Governs Directed Neutrophil Migration in 3D Matrices. *Sci Adv* (2021) 7:eabf3882. doi: 10.1126/sciadv.abf3882
34. Wang WY, Davidson CD, Lin D, Baker BM. Actomyosin Contractility-Dependent Matrix Stretch and Recoil Induces Rapid Cell Migration. *Nat Commun* (2019) 10:1186. doi: 10.1038/s41467-019-09121-0
35. Han SB, Kim JK, Lee G, Kim DH. Mechanical Properties of Materials for Stem Cell Differentiation. *Adv Biosyst* (2020) 4:e2000247. doi: 10.1002/adbi.202000247
36. Franck C, Maskarinec SA, Tirrell DA, Ravichandran G. Three-Dimensional Traction Force Microscopy: A New Tool for Quantifying Cell-Matrix Interactions. *PLoS One* (2011) 6:e17833. doi: 10.1371/journal.pone.0017833
37. Hazlett L, Landauer AK, Patel M, Witt HA, Yang J, Reichner JS, et al. Epifluorescence-Based Three-Dimensional Traction Force Microscopy. *Sci Rep* (2020) 10:16599. doi: 10.1038/s41598-020-72931-6

Conflict of Interest: The authors declare that the research was conducted in the absence of any commercial or financial relationships that could be construed as a potential conflict of interest.

Publisher's Note: All claims expressed in this article are solely those of the authors and do not necessarily represent those of their affiliated organizations, or those of the publisher, the editors and the reviewers. Any product that may be evaluated in this article, or claim that may be made by its manufacturer, is not guaranteed or endorsed by the publisher.

Copyright © 2022 Zhou, Zhao, Yanamandra, Hoth and Qu. This is an open-access article distributed under the terms of the Creative Commons Attribution License (CC BY). The use, distribution or reproduction in other forums is permitted, provided the original author(s) and the copyright owner(s) are credited and that the original publication in this journal is cited, in accordance with accepted academic practice. No use, distribution or reproduction is permitted which does not comply with these terms.